Spray forming of NiTi and NiTiPd shape-memory alloys

Ronald Smith[*a], James Mabe[b], Robert Ruggeri[b], and Ronald Noebe[c]
[a]Materials Resources International, 811 W. Fifth Street, Lansdale, PA 19446
[b]Boeing, Phantom Works, Seattle, WA
[c]NASA Glenn Research Center, Cleveland, OH

ABSTRACT

In the work to be presented, vacuum plasma spray forming has been used as a process to deposit and consolidate pre-alloyed NiTi and NiTiPd powders into near net shape actuators. Testing showed that excellent shape memory behavior could be developed in the deposited materials and the investigation proved that VPS forming could be a means to directly form a wide range of shape memory alloy components. The results of DSC characterization and actual actuation test results will be presented demonstrating the behavior of a Nitinol 55 alloy and a higher transition temperature NiTiPd alloy in the form of torque tube actuators that could be used in aircraft and aerospace controls.

Keywords: Nitinol, NiTi, NiTiPd, shape memory alloys, spray forming, vacuum plasma spraying, actuators, torque tube

1 INTRODUCTION

1.1 Objective

The objective of the work was to demonstrate that Nitinol 55 (NiTi) and NiTiPd shape memory alloys (SMA) could be near net shape formed using vacuum plasma spray (VPS) fabrication methods. In the work, the VPS process was to be used to make more directly fabricated actuation devices, such as torque tubes for aircraft aero-control surfaces as an alternative to cast, forged and machined tubes. Most shape memory alloys (SMA) are made via commercial production processes that consist of casting an alloy ingot followed by rolling/swaging/drawing, all of which can introduce defects and residual stresses. The idea was to eliminate cast/rolling procedures since they are expensive, labor intensive and the product is difficult to machine to final shape. The purpose of the proposed work was to develop a near-net forming process for NiTi and NiTiPd that was more closely controlled and predictable to be able to design and fabricate more reliable, efficient, and cost effective "smart" actuators

1.2 Processing

NiTi based shape-memory alloys (SMA) have emerged as smart "actuator" materials with unique thermal and mechanical properties that are being used to move and/or control aero-surface elements on fixed- and rotary-wing aircraft platforms. The use of such SMA actuators would decrease the cost and decrease the complexity of manufacture for many control elements, while enabling more complex shaping of aero-surface elements leading to enhanced vehicle performance.

A vacuum plasma spray method was optimized for consolidating NiTinol powders into near net shapes to avoid many of the casting defects and inhomogeneties associated with slow solidification rates attributable to cast ingot technology. Powder metallurgy (P/M) investigations had shown that rapidly cooled particles (10 – 200 μm) typically create very uniform, fine grained structures and when pressed and sintered, with the exception of slight increases in the SMAs Martensite start (M_s) temperature, they have retained the shape memory characteristics of the regular cast and formed materials. Vacuum plasma spray (VPS) forming (one of many thermal spray processes) has been shown to be able spray form and consolidate NiTinol powders to high density and to near net shapes by spraying powders onto mandrels.

Figures 1a-1d illustrates the VPS process which was utilized in the investigations. Figure 1a illustrates how the VPS process deposits material onto tubular mandrels and through alternating powder feed lines adds the capability to grade or create layered tubular or flat structures. Figure 1b shows how the VPS process is enclosed in a protective atmosphere

[*] rsmith@materialsreources.com; tel: 215-631-7111x102

Industrial and Commercial Applications of Smart Structures Technologies 2008,
edited by L. Porter Davis, Benjamin Kyle Henderson, M. Brett McMickell, Proc. of SPIE Vol. 6930,
69300S, (2008) · 0277-786X/08/$18 · doi: 10.1117/12.775243

chamber into which a plasma spray gun is mounted. Figure 1c is a schematic of the plasma spray gun, in the chamber, that is used to heat and accelerate injected powder particles. The VPS chamber encloses the spray process and maintains a low pressure (~ 60 – 600 torr) inert gas atmosphere. The mandrel controller penetrates the walls of the VPS chambers and permits multi-axis manipulation of the gun and the substrate to enable controlled deposition for shape control and graded or multi-layered deposits. The chamber and manipulators are typically water cooled to permit long deposition times.

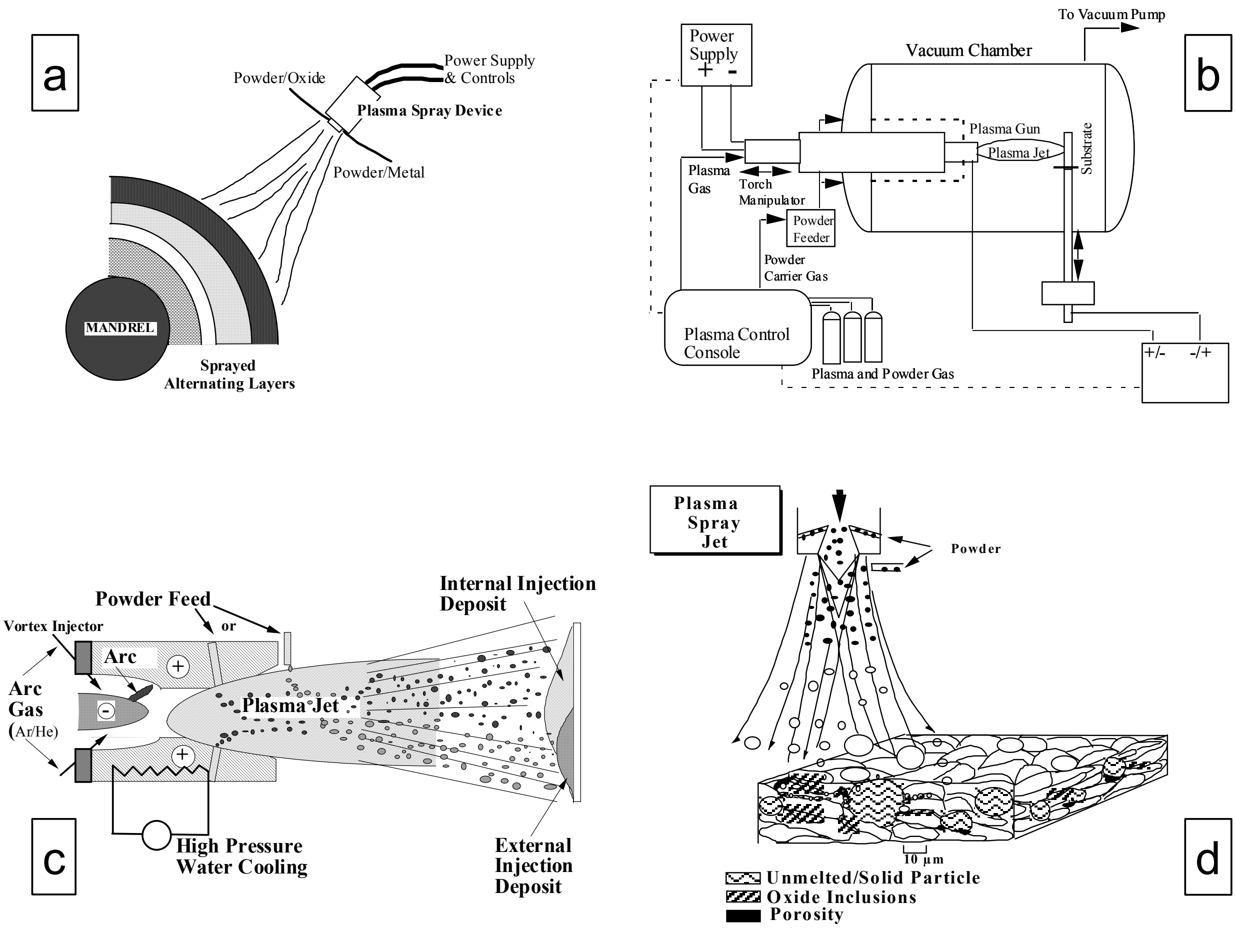

Fig. 1. Schematic illustration of generic thermal spray consolidation processes and equipment: a)spray forming of graded tubular structures, b) the VPS enclosure/chamber, c) a cross section of the plasma spray gun and d) an illustration of the plasma spray deposit.

Figure 1c illustrates how plasma spraying uses electrical (plasma or arc) energy to heat and accelerate finely divided droplets to velocities exceeding 600 m/s. Powder particles are injected into the side wall of the anode/nozzle to entrain the particles into the intensely heated inert gases (normally Ar/He and or H_2). The particles are heated rapidly as they traverse across the heated plasma jet. The jet creates a spray pattern of high temperature particles, where particles are either molten or at least thermally softened. Subsequently, their high velocities cause them to deform on substrate impact into thin lamellar "splats" which conform to the surface. Solidified droplets are thus rapidly built up particle by particle as droplets impact onto the target forming continuous solid layers. The individual "splats" are typically thin (~1-20 µm), such that each droplet cools at very high rates, (near 10^6 K/s for metals) to form extremely uniform, very small grain size, crystalline materials.

1.3 Torque Actuators

The advantages of “smart materials”, such as NiTi (NiTiPd), for use in adaptive structures for control and actuation are well recognized. However; the challenge is to economically and reliably build actuators made from these materials. A major application area for torque actuation is the integration of NiTi tubes or cylinders as hinge pins in “smart hinges”. In these designs the lifting / torque capability of NiTinol has been demonstrated by Boeing and others to be able to lift/rotate large panels that could be flaps and ailerons, doors and other type of panel structures. [1] The advantages of “smart hinges” are that they would be lighter, smaller profile and possibly more reliable than motor actuated devices. By using the hinge pins to actuate, the elimination of many motors and the corresponding electrical power supplies and controllers would greatly reduce weight and save space for other payloads. Systems that would benefit from such “smart hinges” include UAV’s (for flight controls and weapons release), underwater unmanned vehicles, and other manned aero-control and weapons release actuators. Figure 2 shows an active hinge pin concept and demonstration component for aero-surface actuation.

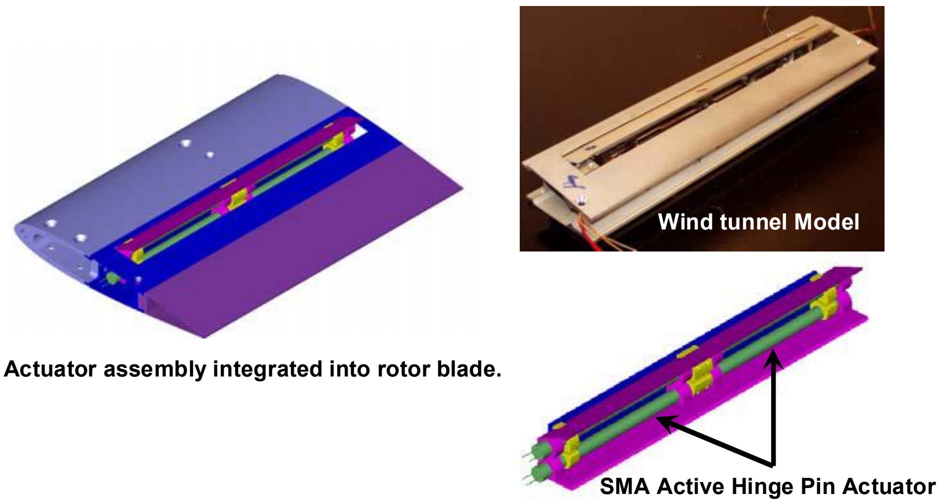

Fig. 2. Active hinge pin actuator for aero-surface control.

2 EXPERIMENTAL PROCEDURES

Two hundred pounds of NiTi powders were ordered from Crucible Research to the following specifications:

Powder Size:	- 270 / + 5 μm
Chemistry:	54.9 Ni 45.1 Ti weight percent (w/o)
Interstitials:	Oxygen < 1,000 ppm: Carbon < 500 ppm

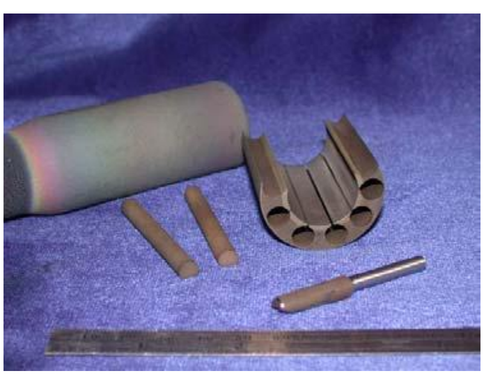

Fig. 3. As-sprayed tubular NiTi shape and EDM machined specimens removed from the

The powders were induction cold hearth melted and directly atomized to minimize handling and contamination. The NiTi and both sets of NiTiPd powders were spray formed into “ingots” of VPS consolidated NiTi and NiTiPd deposits. The ingots were made by loading the powders into controlled atmosphere (argon) canisters that injected these powders into the plasma jet operating inside of a controlled atmosphere chamber, as shown in Figure 1. The powders were sprayed onto steel tube mandrels that were preheated to ~ 800ºC before depositing the powders. Once to temperature, the powder feeders injected the powder at ~ 100g/min into the plasma jet. The melting powders were then deposited onto the surface of the steel tube mandrel as the jet transversed axially over the tube as the tube was rotated. Figure 3 illustrates the tubular NiTi deposits that were made onto to the steel tube mandrel. Deposit thicknesses were ~ 10-12mm, enough for round bar and beam to be made from. All metallographic samples, DSC samples and cantilever beams were made from such deposits, shown in Figure 3.

NiTi actuator tubes were made by directly depositing onto ~ 150mm L by 6mm D rod to produce the net shape spray formed NiTi torque tubes that were tested in torsion. The NiTiPd torque tubes, to conserve the more expensive NiTiPd powders, however, were spray formed as shown in Figure 2, machined into rod then drilled to produce test torque tubes. Torque tubes were made to 125mm x 5 mm OD and 3mm ID then a pin was inserted into the tube end to hold the attachment hex nut.

After deposition, the VPS deposits required heat treatment to interdiffuse the sprayed structures and to homogenize the compositional variations that might come from differing local deposit conditions and to assure interparticle bonding. Heat treatments include:

1. 890°C - 1 hour- quench / 350C - 40 min. quench
2. 890°C - 1 hour- Ar quench
3. 1120°C - 1 hour quench / 350C - 40 min. quench
4. 1120°C - 1 hour -Ar quench

Characterization of deposits included mounting and polishing both the as-deposited materials, followed by optical and/or scanning electron microscopy (SEM) in both the as polished and in the etched conditions, where etching was used to elucidate the structure of the deposited materials. Deposit "wet" chemistry was conducted along with interstitial gas analysis for N_2 and O_2.

Deposit properties were measured in three different ways to determine shape memory behavior and properties; 1) differential scanning calorimetry (DSC), 2) cantilever beam and 3) actual torque tube cycling.

DSC testing was used to identify the critical temperatures associated with phase changes such as the martensite start (M_s) martensite finish (M_f), austenite start (A_s) and austenite finish (A_f) via their exo- and endo-therms. Martensite was the lower temperature phase for the NiTi and NiTiPd and represents a lower symmetry and more complex crystallographic structure than the higher temperature austenite phase which was a simpler cubic structure. The martensite structure for the NiTi alloy was monoclinic, while that for NiTiPd alloy was orthorhombic.

Cantilever beam testing was conducted as shown in Figure 4. The beam samples were VPS formed and rough machined from the deposited ingot (Figure 3) and then homogenized at 890 °C for 2 hours and aged at 500 °C for 5 hours, in vacuum, with a helium quench before final machining to dimensions of approximately 100 mm x 6 mm x 2mm. A photo of a cantilever beam VPS test specimen is shown in Figure 5. The rectangular cross section beams were then subjected to various constant loads while the temperature environment of the beam and the instrumentation (for measuring load and deflection) were cycled (heated and cooled) in a furnace.

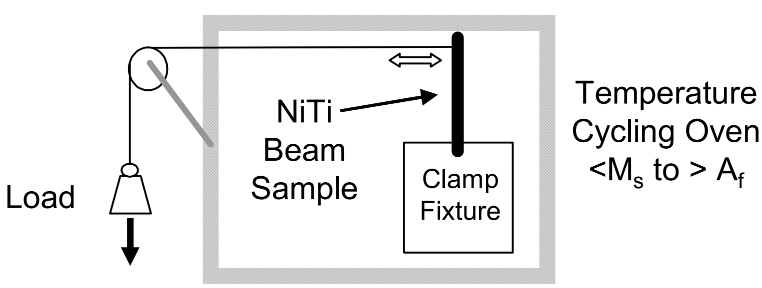

Fig. 4. Schematic illustration of the cantilever beam test rig.

The beam samples were Vacuum Plasma Spray (VPS) formed and rough machined from the deposited ingot (Figure 3), the beam blanks were homogenized at 890C for 2 hours and aged at 500C for 5 hours, in vacuum, with a helium quench before final machining. A photo of a cantilever VPS test beam is shown in Figure 5.

Fig. 5. Picture of a typical cantilever beam test specimen.

Torque tube testing and actuator performance was determined using a test set up as shown in Figure 6. This test used a pulley system and dead load to provide a constant pure shear load on the VPS tubes. In this test, spray formed tubes were pinned to hex nuts, see Figure 6, and a hex nut was fixed onto the end of the spray formed and machined tube to engage the load train. The tubes were then placed under a torque load with an applied dead load on the pulley and heated by electrically operated, thermo-electric modules (TEM) and cooled through a heat sink. The unit had heater/cooler controls that permitted the torsion cycling of the torque tube under various preload conditions. During testing, strain as a function of temperature over a series of loads was measured for up to 1,000 thermal cycles.

The NiTi torque tubes were deposited directly on smaller mandrels to form the ~ 125mm long x 10 mm ID x 5 mm ID tubes while the NiTiPd torque tubes were made in the same manner as the cantilever beams, e.g., made from round bar machined from sprayed ingots. The sprayed tubes were cut to length , the ID were drilled to remove the steel tube mandrels, the blanks were heat treated (890ºC- 1 hour, followed by 550ºC for 3 hours, in vacuum) then the final OD were machined before drilling pin holes and inserting the hex heads, as shown in Figure 7.

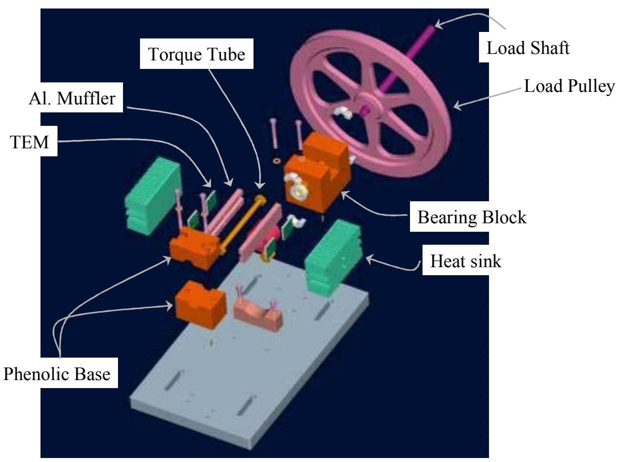

Fig. 6. Schematic illustration of the shape memory torque tube test rig.

Fig. 7. Picture of a VPS formed NiTi shape memory tube for torque tube testing.

3 RESULTS & DISCUSSION

3.1 Deposit Chemistry

Two independent chemical analyses were performed on the as-received 55NiTi powder as well as on the deposit after spraying and the results are shown in Table 1. The results indicate that after VPS processing the composition was close to the original powder composition, with some increases in O_2 and N_2 content and no change in carbon.

Table 1 Chemical Analyses of the As-Received Powders and VPS Deposited 55 NiTi (wt.%)

	Powders (Crucible)	Powders Stork	LTI (VPS)	VPS NiTi Deposit
Element	Wt%	Wt%	Wt%	Wt%
Ni:	54.7	55.41	54.40	55.56
Fe:	<0.005	N/A	0.001	1.15
H:	N/A	0.001	N/A	N/A
Cu:	<0.005	N/A	N/A	N/A
Cr:	<0.005	N/A	N/A	N/A
C:	0.011	N/A	0.008	.11
O:	0.066	0.06	0.101	.23
N:	0.003	0.002	0.025	.006
Ti:	Bal. (45.22)	44.53	45.17	42.89

NiTiPd powders were also produced by Crucible and were similarly VPS deposited. Their Chemistries are shown in Table 2 and 3. The VPS deposits shown in Table 2 had much higher oxygen and a Ti/ (Ni+Pd) ratio that was less than ideal for maximizing transformation temperatures. Later DSC analyses confirmed that the transition temperatures were not as high as planned. For maximum transformation temperatures the Ti/(Ni,Pd) ≥ 1**.** Consequently a second set of powders with improved Ti/(Ni,Pd) ratio was produced and its composition is shown in Table 3. The powders showed good agreement with the new aim composition; however, the oxygen content was higher than expected. At this level there was some concern that the final VPS oxygen content might have been high enough to affect the SME behavior, but DSC showed this particular alloy was more tolerant of oxygen content. As Table 3 indicates, the modified VPS NiTiPd alloy had a measured oxygen content of 2,800 ppm. Table 3 also shows the pre-VPS powder to be higher in at. % Ti than the aim of 51 at.% with the nickel and the Pd slightly lower.

Table 2 Chemical Analyses of the Original NiTiPd Powder and VPS Deposited Material (wt.%)

	Powder (Crucible)	Powder (Stork)	LTI (VPS)
Element	Wt%	Wt%	Wt%
Ni:	27.6	28.8	27.43
Fe:	0.03	N/A	0.058
H:	N/A	0.001	N/A
Pd:	33.8	33.92	34.4
Cr:	<0.01	N/A	N/A
C:	0.013	N/A	0.011
O:	0.056	0.05	0.14
N:	0.033	0.026	0.049
Ti:	Balance (38.46)	37.12	38.24

Table 3. Analyses of the Modified NiTiPd Powder and VPS Deposited Material (at.% and wt.%)

	Ni	Ti	Pd	O	C
Powder (actual)					
a/o	28.32	51.79	19.89		
w/o	26.42	39.43	33.64	2100 ppm	230 ppm
VPS (actual)					
a/o	26.92	52.69	20.39		
w/o	25.04	39.99	34.38	2800 ppm	500 ppm

The aim composition for the second heat of modified NiTiPd powders (Table 3) used for VPS deposition had an aim Ti content of 51 at.%, higher than the nominal 50 at.% with the expectations that some of the Ti would be tied up by reaction with the oxygen during both powder atomization and VPS deposition.

3.2 Deposit Structure

Metallographic samples were prepared from a set of VPS NiTi deposits and, as shown in Figure 8a (as-polished cross section) there was less than 2% porosity with no visual indications of excessive deposit oxidation. Figure 8b shows the same cross section and magnification as Figure 8a, after etching the sample in a dilute solution of hydrofluoric and nitric acids in water to bring out the as-sprayed layer structure. It can be seen that the layers are well-adhered to each other and free from any excessive oxide. There were also very few unmelted particles as seen in the higher-magnification view of the etched deposit in Figure 8c.

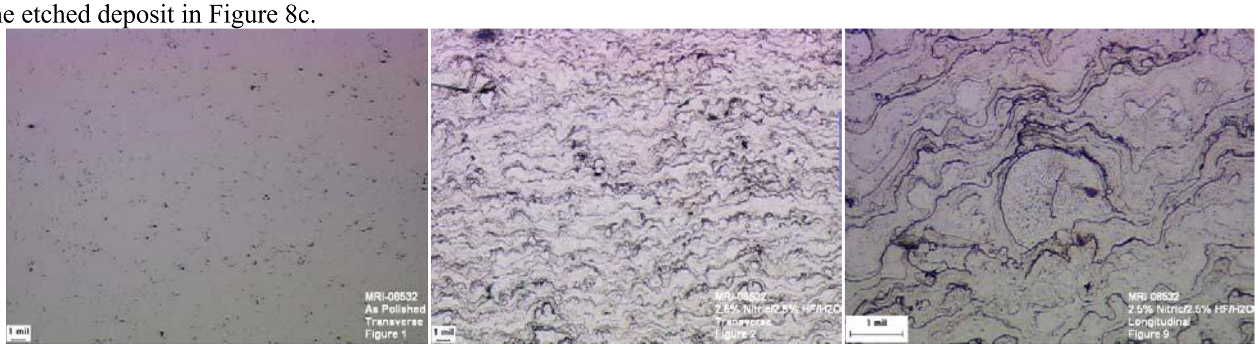

(a) (b) (c)

Fig. 8. As-Polished transverse metallographic cross section of VPS NiTi(55) a) as polished 200x, b) etched 200x and c) etched at 1,000x.

In addition to optical metallography, detailed scanning electron microscopy (SEM) and transmission electron microscopy (TEM) was performed on the original VPS processed NiTiPd alloy and representative results are shown in Figure 9. Similar to the 55NiTi alloy, the NiTiPd alloy structure consisted of extremely wavy splat boundaries and approximately 1-2 vol.% porosity (Figure 9a). More detailed analysis of the splat boundaries including electron diffraction analysis of the particles shown in Figure 9c indicate that the boundaries consisted of individual particles of $Ti_4(Ni,Pd)_2O_x$ rather than a continuous oxide skin. Between the boundaries both submicron particles of $Ti_4(Ni,Pd)_2O_x$ and TiO_2 were observed.

Metallographic analysis of the modified NiTiPd alloy after VPS processing indicated that porosity was essentially eliminated in this alloy and that oxide layering at the interparticle boundaries was minimal. The etched structures showed a relatively equiaxed NiTiPd grain structure and fine grain size of 1 -5 µm, similar to the original NiTiPd alloy. After homogenization and aging (890ºC- 1 hr in vacuum, cooled to R.T. followed by 700ºC- 1 hour in vacuum) the grain size remained uniform at ~ 5 µm and delineated by the original splat interfaces.

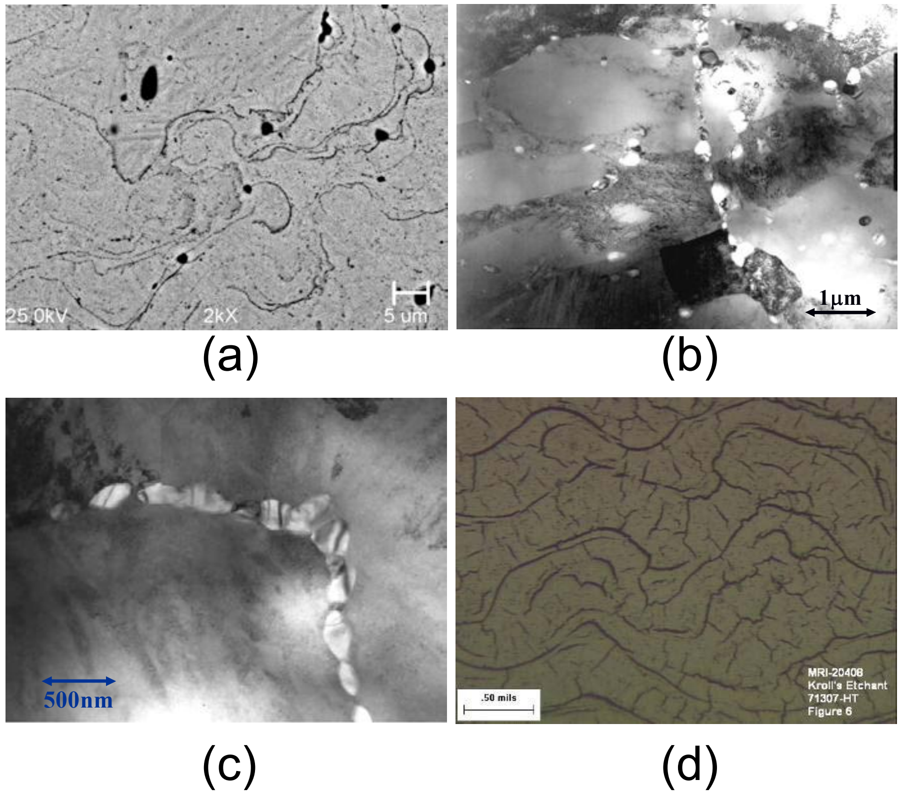

Fig. 9 Microstructural characterization of the original VPS NiTiPd alloy. a) SEM micrograph showing splat boundaries and occasional porosity and TEM brightfield image of b) the general structure of the alloy consisting a fine grain size and sub-micron particles with a splat boundary running down the center of the image and c) higher magnification view of a splat boundary composed of individual Ti4(Ni,Pd)2Ox particles and d) 1,000x polished cross section.

3.3 Differential Scanning Calorimetry (DSC)

DSC results on both the NiTi and the NiTiPd are presented in Figures 10 and 11, respectively, and show the typical exo- and endotherms indicative of the martensitic transformation. The basic phase transition temperatures, e.g., M_S, M_F, A_s and A_f are also designated on each plot. The results indicate that NiTi and NiTiPd can be processed by VPS and post heat treatment with transformation temperatures comparable to that of cast and wrought materials. Figure 10 show the DSC results on both as-deposited and homogenized material (890 ºC for two hours). Homogenization is shown to both sharpen the transformation peak and increase the transformation temperature.

Figure 11a-b shows the DSC results of the second heat of modified NiTiPd deposited by VPS. The results indicate that material produced by this technique exhibits very good transition temperatures that met the requirement of a minimum M_f temperature of 100 °C and the transition energy was deeper and sharper than the cast alloy, indicating good SME behavior. The DSC results also indicated that the higher temperature shape memory behavior that was being sought, was achieved in both the as-deposited (Figure 11a) and post deposit heat treated (Figure 11b) NiTiPd alloy. Post deposit heat treat, as in the VPS NiTi alloys, also improved the transformation behavior, sharpening the transformation and increasing the transformation temperatures by 4-5 ºC.

In the investigations of NiTiPd VPS materials, rapidly cast alloy buttons were used to identify the optimum Ti.(Ni,Pd) ratios and Pd concentrations for VPS processing. Figure 12 summarizes these rapid quenched arc-melted button results showing that a peak in transition temperature occurs with the aim composition of 50.2 a/o Ti. The figure also shows the initial VPS data (star data points), indicating that the arc cast, quenched and heat treated NiTiPd alloys closely resembled the behavior of the VPS materials.

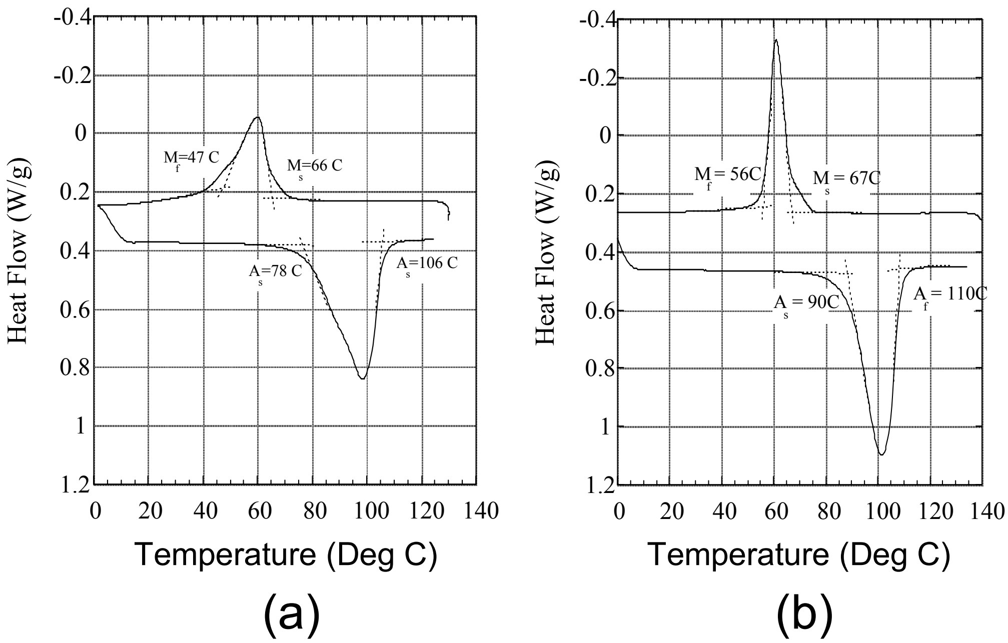

Fig. 10. DSC results for 55NiTi material in the a) as-sprayed condition and b) after homogenization at 890°C for 2 hrs.

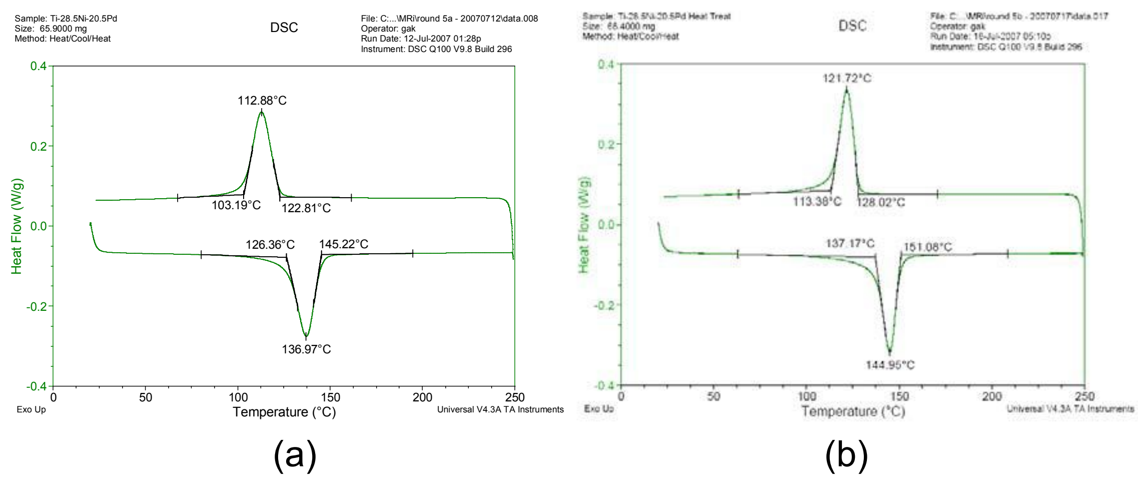

Fig. 11. DSC results for a 51Ti-28.5Ni-20.5 Pd a/o alloy in the a) as-sprayed condition and b) after homogenization.

Figure 13 shows that in general the transformation temperatures, M_f and A_f, increase with increasing Pd content. Heat treatment on the quenched specimens raised the A_f temperature slightly and decreased the M_f temperature while sharpening up and deepening the transition as observed in the DSC scans. However, the data for the 20Pd containing alloy was not consistent with the bulk of the data underlying the difficulty in working with alloys with such extreme sensitivity to composition.

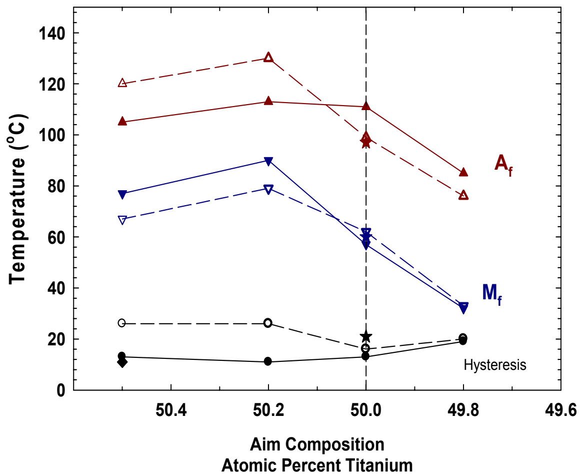

Fig. 12. Transformation temperatures as a function of Ti content for arc cast-quenched and heat treated NiTiPd alloys. Solid symbols/solid lines represent as-quenched material. Open symbols/dashed lines represent quenched plus homogenized material and the stars are the results from the first heat of VPS NiTiPd after VPS processing, homogenization, and aging.

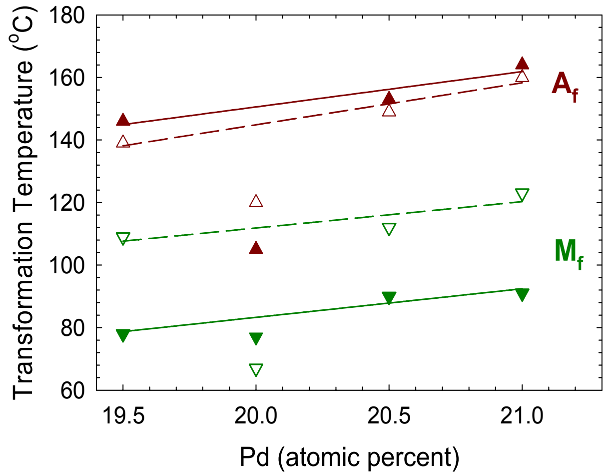

Fig. 13. Transformation temperatures as a function of Pd content for arc cast-quenched and heat treated Ni49.5-xTi50.5Pdx alloys. Solid symbols/solid lines represent as-quenched material and the open symbols/dashed lines represent quenched plus homogenized material. Note that the data for 20Pd alloy is not consistent with the balance of the alloys and exhibits significantly lower transformation temperatures, another indication of the difficulty in controlling composition over such a narrow range in these materials.

3.4 Cantilever Testing

The hysteresis loop for five VPS formed beams after approximately 200 cycles at a nominal load of 85 MPa is shown in Figure 14. All were homogenized at 890ºC, but were then aged over a range of temperatures and times as indicated in the figure. Overall the results for all of the beams are similar, particularly the transition temperatures and hysteresis loop characteristics. Beam #MRi-05-B2 was initially cycled at a low load of only 36 MPa which accounts for its lower overall strain values and lower unrecovered strain. In Figure 14 the total dynamic tip displacement varies by only 0.5% for all of the beams, this level of variation is not uncommon for SMA materials.

Transition temperatures for a VPS formed beam with no aging after homogenization were determined from initial low load cantilever beam testing. These transition temperatures are compared to the "unloaded" DSC measured transition temperatures in Table 5. The lower transition temperatures on the "loaded" beams was attributed to thermal mass and loaded conditions of the beam test, compared to the low thermal mass DSC tests.

Typical thermomechanical cycling data for a VPS formed beam is shown in **Figure 15.** This beam was homogenized at 890°C and then aged at 500°C for 4 hours. The load was varied over the course of the test. The reduction in creep rate is seen over cycles 400 - 600 after cycling at a much higher stress level. The final approximately 25 cycles were done with a very small applied stress and the 2-way SME is clearly evident. Previous research has shown very similar behavior in wrought SMA actuators. [2-3].

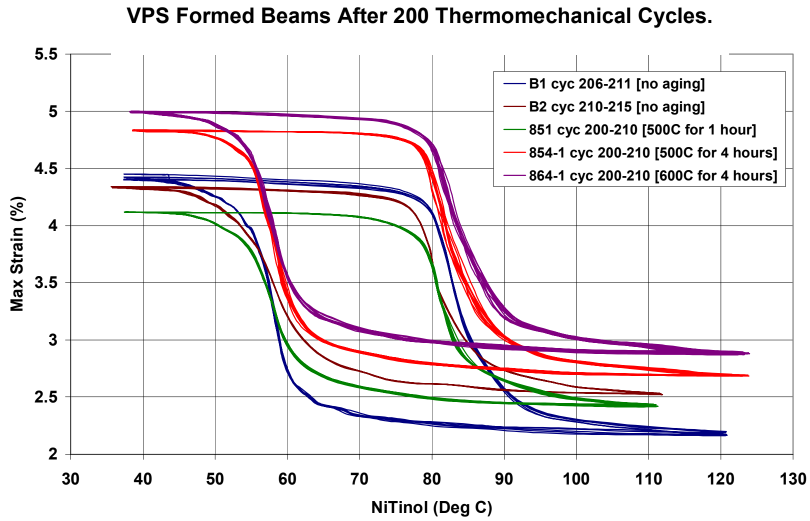

Fig. 14. Strain vs. Temperature Hysteresis loops for VPS Formed Beams after 200 Thermomechanical Cycles.

Table 6. Transition Temperatures Beam MRI-B1

	Cantilever Beam	**DSC**
A_s (Deg C)	80	90
A_f (Deg C)	95	110
M_s (Deg C)	65	70
M_f (Deg C)	50	55

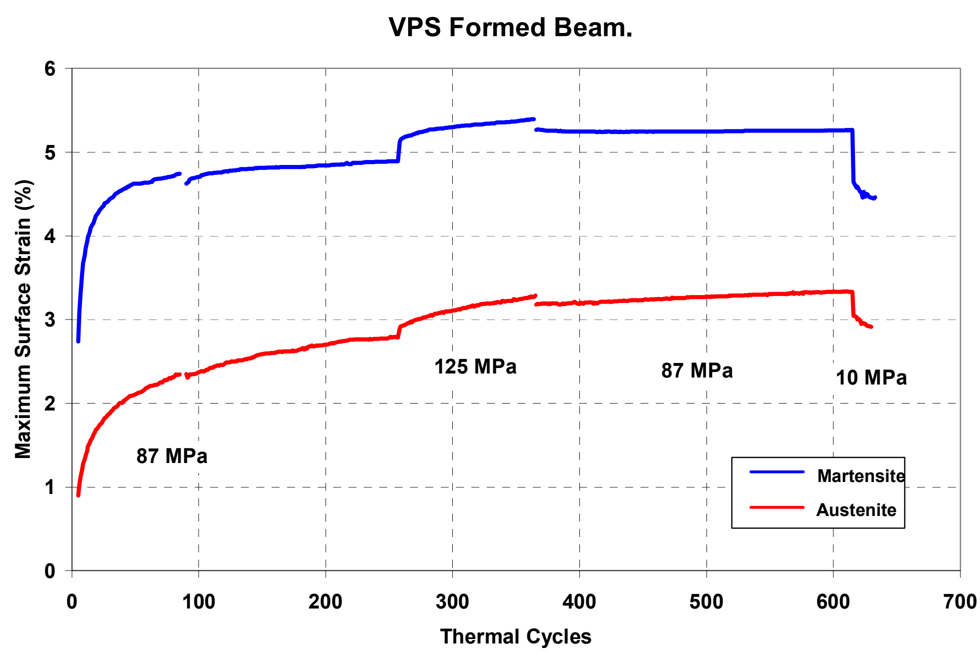

Fig. 15. Austenite and Martensite strain vs. Cycle Count for VPS Formed Beam

A comparison of the wrought cantilever beam vs. a VPS NiTi cantilever beam is shown in Figure 16. The wrought bar beam is the red trace (lower curve) and the VPS specimen is the blue trace. The transition temperatures were similar; however, but there were clear differences in the hysteresis loop characteristics. The particular wrought bar was aged at a much lower temperature than the VPS specimens. Previous testing has shown that higher aging on the wrought bars will generate a hysteresis loop more like the VPS specimens [4]. The conclusion from this and other comparisons was that VPS and wrought NiTi (55) alloys had similar shape memory effect behavior, but that the VPS materials send to stabilize quicker during stain cycling.

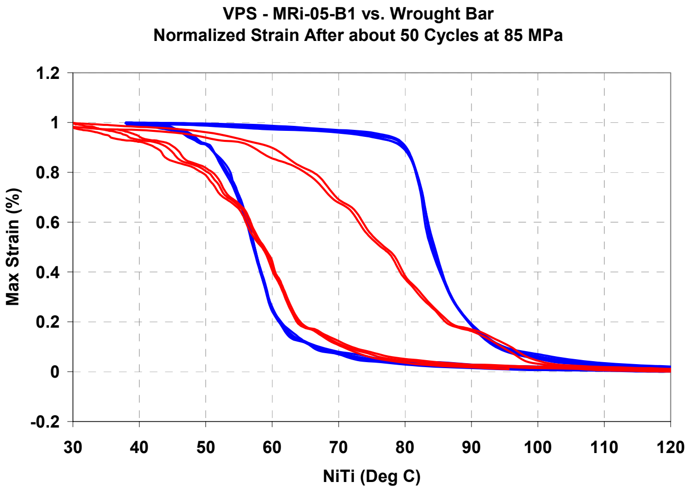

Fig. 16. Comparison of torsion tube thermomechanical testing NiTi (55) wrought and VPS specimens

The results of cantilever beam testing of selected Ni (27.4) Ti (38.2)Pd(34.4) (w/o) beams are shown in Figures 17a-b. These figures show the hysteresis loops for the beams at the beginning and ending of thermal-mechanical cycling**.** It was observed that the material's properties and characteristics were consistent and repeatable and was comparable to the NiTi(55) results; however with increased transition temperatures over those of VPS NiTi(55) alloys. It can be seen that the transition temperatures were not as high as expected and led to further compositional developments, varying Ni:Ti ratios and Pd concentrations. The transition temperature for a more optimal NiTiPd composition were identified by DSC testing, as shown in Figure 11, but this alloy had not been tested using the cantilever beam test.

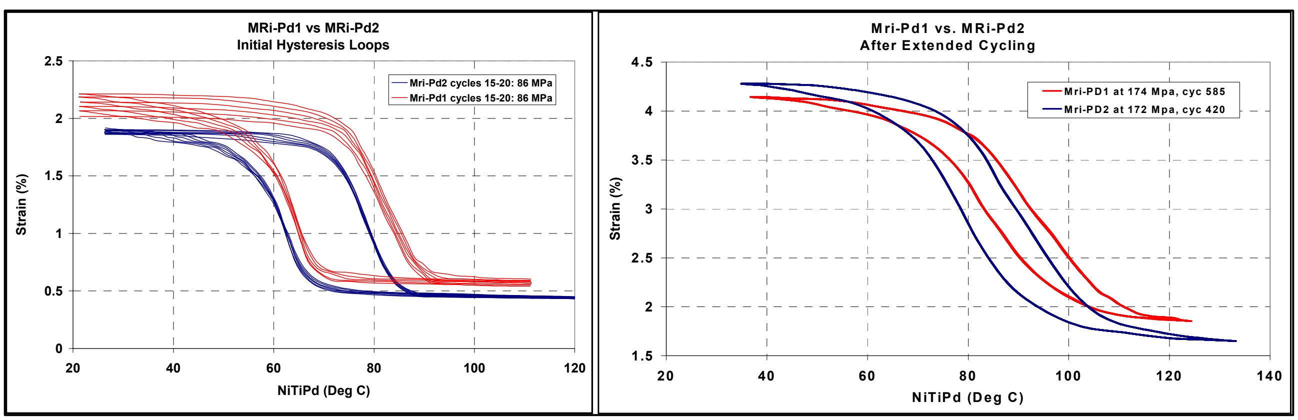

Fig. 17. Summary of strain temperature hysteresis loops measured during cantilever testing VPS NiTi(55) Beams.

3.5 Torque Tube Testing

Torque tubes fabricated from VPS formed 55NiTi material had measured properties similar to what was observed in the 55NiTi beams. Typical data for VPS tubes and wrought tubes are shown in Figure 18.

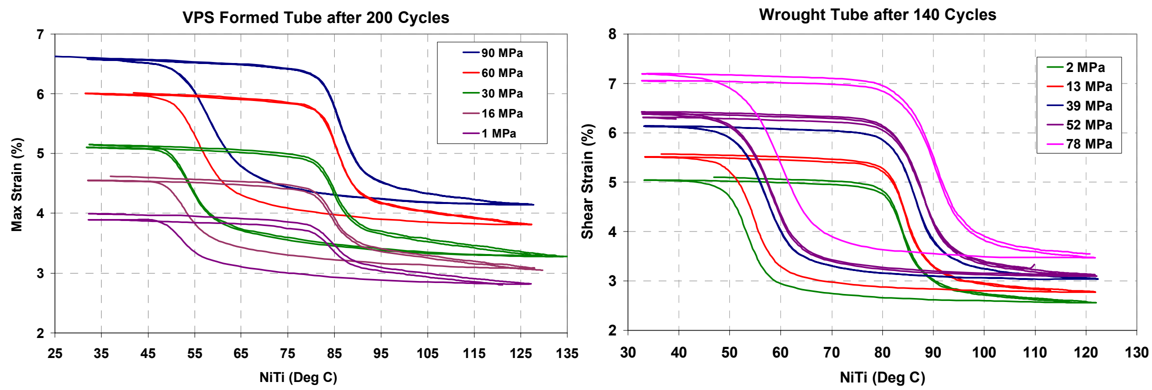

Fig. 18. Stain vs. Temperature Hysteresis Loops for VPS and Wrought Tubes.

The hysteresis loops for a VPS NiTi(55) tube tested over a range of applied loads after 1180 cycles is shown in Figure 19a. The increase in transition temperature with increased loads was especially evident in Ms. Transition temperatures and loads from the same data are plotted in Figure 19b. It was clear that the Martensite temperatures was more sensitive to load, and reportedly similar to cast and wrought materials.

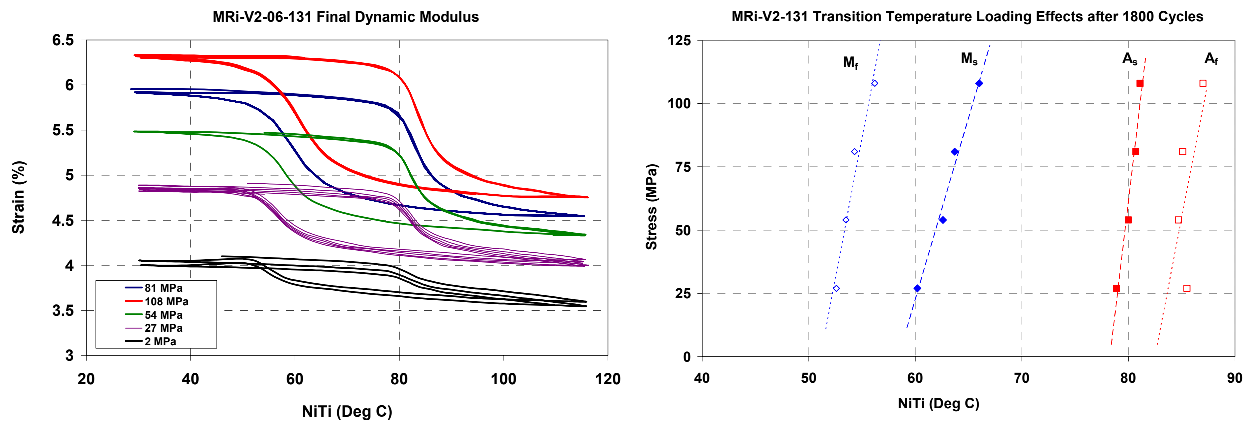

Fig. 19: Loading Effects for VPS MRi-V2-06-131 after 1200 Cycles

Typically for actuator design, SMA component characteristics and performance can be evaluated in two ways. The first method is essentially a measure of the materials Young's modulus. By varying the applied stress and measuring the strain while maintaining a constant temperature at temperatures both above A_f and below M_f. The Young's modulus can then be calculated from the slope of the stress vs. strain curve. The second method, designated the Transformation Modulus, involves thermal cycling the component under varying loads and plotting the fully Austenite and the fully Martensite strains vs. the applied stress for that particular cycle. While both the Young's Modulus and Transformation Modulus were important properties, for actuator design the SMA's Transformation Modulus was is more indicative of performance in an actuator. The Transformation Modulus captures not only the change in static modulus between the Austenite and Martensite forms, but also captures the shape memory effect, including two-way, and the significant shift in the material properties that occurs during transition. The initial and final Transformation Modulus for the VPS formed material and wrought N55NiTi material is shown in Figure 20 and Table 7. There is typically a wide range of measured Transformation Modulus in SMA materials. The Transformation Modulus of both the VPS and wrought materials varied somewhat, but are within the range of what might be expected for SMA components with varying fabrication and conditioning histories. However the two-way SME for the wrought specimens was significantly higher.

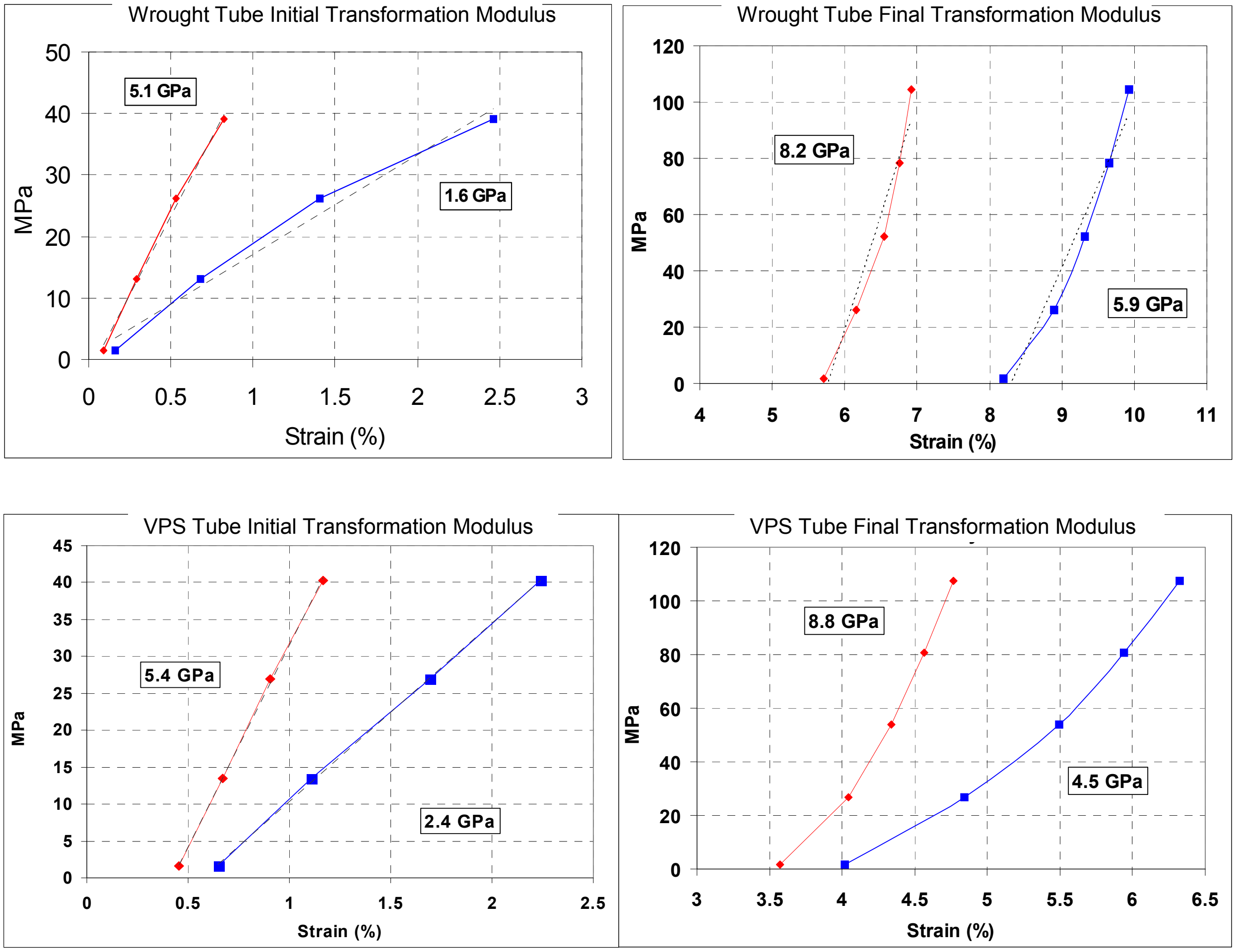

Figure 20. Transformation Modulus for VPS and Wrought Tubes

Table 7: VPS Tubes Compared to Wrought Tube Results

		Dynamic Modulus (GPa)		
	Cycles	**Martensite**	**Austenite**	**Two-way (%)**
MRi-V2-06-131	1200	4.5	8.8	0.5
MRi-V2-129	200	3.4	6.6	1.3
S25	350	5.9	8.2	2.5

Due to oxide contents and non-optimal Ni:Ti ratios of the initial Ni (27.4) Ti (38.2)Pd(34.4) (w/o) deposits had lower than expected ductility. This low ductility led to notch sensitivity and reduced the reliability of torque tubes tests. Therefore the data is not reported here since it was not representative of VPS NiTiPd could achieve.

SUMMARY OF RESULTS

The investigation and reported results have demonstrated that VPS-NiTi and NiTiPd shape memory alloy torque actuator tubes can be produced and have SME behavior that compares well to wrought NiTinol 55 alloys. For NiTi(55) the transition temperatures and strain ranges were similar but different enough that there would need to be some adjustments made to actual VPS formed NiTi torque actuators. Specifically, i) As-deposited and homogenized VPS-NiTi materials were able to achieve SME behavior nearly equivalent to wrought DSC, ii) mechanical measurements on VPS-NiTi showed the following transition temperature ranges Mf= 50-52ºC, Ms=58-62ºC, As=82-85ºC and Af=87-90ºC. These are close to the same transition temperature ranges of wrought Nitinol 55, iii) Cantilever beam testing showed strain ranges and other mechanical behavior that deviated at bit from typical wrought Nitinol 55, however, when the wrought materials were aged a bit higher the beam hysteresis data was again similar, iv) Static and dynamic modulus of the VPS-NiTi was slightly lower but similar to wrought Nitinol 55, v) VPS formed NiTi torque tubes were able to be made by depositing onto tube mandrels, machining out the steel ID mandrel, followed by homogenization heat treatment and then turning the OD to the specified dimensions, vi) VPS-NiTi materials were found to creep less than wrought Nitinol 55 and were found to stabilize and train sooner and that torsion testing on VPS-NiTi(55) and wrought Nitinol 55 torque actuator tubes yielded similar performance.

The results of the VPS-NiTiPd work demonstrated the capability of the VPS process to form NiTiPd shapes from powders but initial, non-optimized composition [Ni (27.4) Ti (38.2)Pd(34.4) (w/o)] showed that expected behaviors were not achieved. First, the A_f transition temperatures did not achieve ~ the expected 130ºC. This lower than expected transition temperature was likely due to compositional effects from powder and VPS processing, where oxygen interacted with titanium, thus shifting the Ti/(Ni+Pd) Ratio. Additionally, during the testing of the torque tubes, the VPS-NiTiPd materials failed at lower applied stresses and early in cycling. The failure was found to be related to crack defects that developed at the surfaces of the machined tubes that propagated during torsion testing. This result indicated that the "off composition VPS-NiTiPd materials were notch sensitive.

Based on the poor transition temperature response of the initial VPS NiTiPd and on it low toughness an effort to optimize the NiTiPd composition was completed. The work aimed at offsetting the influence of oxygen and other gas interstitials on the final NiTiPd composition and structure. NiTiPd alloy transition temperatures are very sensitive to the Ti levels and to the Ti/(Ni+Pd) ratio. This work showed there was an increase in the transition temperature of rapidly recast NiTiPd with increasing Pd content from 19.5 – 21 a/o. A target NiTiPd composition for VPS powder was selected having a higher Ti content than the measured arc cast materials. The candidate VPS alloy was selected as 28.5Ni51Ti20.5Pd. VPS deposited material of this composition was successfully made into powder; however, oxygen contents were over 2,000 ppm due to the melting and atomization process. VPS deposition of the powders yielded a further increase in oxygen content to 2,800 ppm. The VPS deposited NiTiPd, despite the high oxygen content, had very good SME based on transition temperatures determined by DSC measurements. The as-deposited and the heat treated materials both showed transition temperatures that were between 110 - 150ºC. However the project was stopped before any mechanical data could be determined for the latest heat of NiTiPd VPS material.

ACKNOWLEDGEMENTS

The authors would like to recognize the generous support of the SBIR offices of NAVAIR and NASA under DoD contract N68335-04-C-0191 and NASA contract NNC07QA121P. The results and data contained in this paper are also subject to the SBIR Data rights clauses of the referenced contracts. R. Noebe would also like to recognize support of the NASA Fundamental Aeronautics Program through the Subsonic Fixed Wing Project and A. Garg for performing electron microscopy on the NiTiPd VPS material.

REFERENCES

1. L. Gravatt, J. Mabe, G. Bushnell, E. Gutmark, R. DiMicco, and C. Harris "Shape Memory Alloy Actuators for Deployable Rotor Blade Aerodynamic Devices", 46th AIAA Aerospace Sciences Meeting and Exhibit, Reno, AIAA-2008-1451, Nevada, Jan. 2008.

2. J. Mabe, R. Ruggeri, F. Calkins, "Characterization of Nickel-rich NiTinol Alloys for Actuator Development", The International Conference on Shape Memory and Superelastic Technologies, Pacific Grove, CA, May 7-11, 2006

3. J.H. Mabe, R.T. Ruggeri, E. Rosenzweig, and C. Yu, "NiTinol Performance Characterization and Rotary Actuator Design", SPIE Smart Structures and Materials 2004, SPIE-5388-11, San Diego CA, March 2004.

4. J.H. Mabe, E. Rosenzweig, and C. Yu, "A comparison of the DSC measurements of shape memory alloys and the material's thermal characteristics in a large scale actuator", SPIE Smart Structures and Materials 2006, SPIE-6170, San Diego CA, March 2006.